Clays and Clay Minerals, Vol. 56, No. 6, 711–729, 2008.

CLAY MINERALS IN BASALT-HAWAIITE ROCKS FROM MURUROA ATOLL (FRENCH POLYNESIA). I. MINERALOGY

ANTOINE MAS, ALAIN MEUNIER*, DANIEL BEAUFORT, PATRICIA PATRIER, AND PATRICK DUDOIGNON
University of Poitiers, HYDRASA INSU-CNRS, 40 avenue Recteur Pineau , 86022 Poitiers Cedex, France

Abstract—Clay minerals in chilled or brecciated margins (altered glass) and massive inner crystalline parts (mesostasis) of three basalt-hawaiite bodies from Mururoa Atoll (French Polynesia) have been studied in order to compare their chemical and mineralogical compositions. Polyphase assemblages comprise di- and trioctahedral phases, both of which consist of non-expandable layers (chlorite, celadonite) and two types of expandable layers (saponite and Fe-rich smectite or 'nontronite-like' material). The presence of the Fe-rich clays is supported by the presence of the X-ray diffraction 060 peak at 1.51−1.52 Å and of the infrared absorption bands at 875 and 822 cm^{-1} (Fe^{3+}-Al-OH and Fe^{3+}-Fe^{3+}-OH groups, respectively). The chemical composition of the Fe-rich smectites does not fit with the theoretical nontronite field. The layer charge averages 1 per Si_4O_{10} making these Fe-rich smectites close to 'celadonite-type' clays. This could explain the presence of mixed-layer celadonite-smectite. Plotted in an M^+/4Si *vs.* Fe/sum octahedral cations diagram, the chemical compositions of clay minerals in the mesostasis form a continuous field limited by the celadonite−high-charge nontronite-like smectite and chlorite end-members. The clay assemblages are different from those formed in hydrothermal systems or low-grade metamorphic conditions which are characterized by the sequence: saponite → randomly ordered chlorite-smectite mixed-layered minerals (MLMs)→ corrensite → chlorite. The systematic presence of Fe-rich clays either in the altered chilled margins or in the massive inner parts of the basalt-hawaiite bodies (high-charge nontronite-like smectite and mixed-layer nontronite-celadonite) makes the Mururoa seamount a potential terrestrial analogue for Mars surface exploration.

Key Words—Basalt, C-S, Celadonite, French Polynesia, Glass, Mesostasis, Mururoa, Nontronite, Vesicle.

INTRODUCTION

Clay minerals in basaltic rocks have been studied widely, from basalts which are in weathered zones to heavily metamorphosed basalts, in both the continental and oceanic crusts (Alt, 1999; Meunier, 2005, among others, and references therein). Whatever the geological situation, clay minerals are classically considered to result from the alteration of pre-existing silicates. The most unstable silicate components (olivine and volcanic glass) are commonly replaced by clay minerals even in apparently unaltered basalt rocks. Most often, clays are associated with zeolites or carbonates in zoned deposits, sealing fractures and vesicles. The crystal-chemical properties of clays change with temperature and water/rock ratio forming the following sequence: saponite → randomly ordered mixed-layer chlorite-smectite minerals (R0 C-S MLM) → corrensite → chlorite (Table 1). This trioctahedral phyllosilicate sequence is used as a marker of fluid-rock interactions in hydrothermal or low-grade metamorphism conditions in basalt flow series because the proportion of chlorite layers changes from 0 to 100% with increasing grade. Besides, the chemical composition changes concomitantly. Schmidt and Robinson (1997) demonstrated the similarities in the MgO/(MgO+FeO) ratio (X_{MgO}) of saponite, corrensite, and chlorite, on one hand, and the X_{MgO} of the whole rock, on the other. This militates for a continuous crystal-chemical change with increasing temperature.

The sequence concept, based on trioctahedral clay minerals, is not only established at the scale of basalt flow piles, but is also consistent with the mineral zoning observed inside single flows. Neuhoff *et al.* (1999) showed that such mineral zoning depends on the permeability-porosity contrast between vesicular and massive levels. However, several questions arise in the interpretation of the trioctahedral phyllosilicate sequence in spite of its apparent consistency. The first question concerns the variation in X_{MgO} which is used as an indicator of thermally controlled changes in solid solutions of trioctahedral Mg-bearing phyllosilicates. The temperature dependence of X_{MgO} is implicitly based on the assumption that Fe ions (the oxidation state of which is generally unknown) are not shared with other coexisting mineral phases in the system. In fact, celadonite, a dioctahedral Fe-bearing clay species, is frequently observed in basalts. However, this mineral is considered to be a product of an earlier alteration event and to remain stable during the development of the trioctahedral reaction sequence. Is celadonite the only Fe-bearing clay species in basalts or are others also present? To address this question requires a detailed

* E-mail address of corresponding author:
alain.meunier@univ-poitiers.fr
DOI: 10.1346/CCMN.2008.0560611

Table 1. Review of the mineralogical composition of clay assemblages formed in hydrothermal systems and under low-grade metamorphism conditions.

Clay mineral assemblage	Geological environment	Reference
Celadonite + silica Chlorite/smectite (Ch20/sm80 to Ch80/Sm20) Zeolites	Low-grade metamorphism	Neuhoff *et al.* (1999)
Smectite Corrensite Chlorite	Low-grade metamorphism	Schmidt and Robinson (1997)
Smectite Chlorite/smectite R0 Corrensite Chlorite	Low-grade metamorphism	Bettison and Schiffman (1988)
Di-smectite + saponite Chlorite/smectite (Ch20/sm80) R0 Corrensite	Hydrothermal alteration	Schiffman and Fridleifsson (1991)
Celadonite, saponite Celadonite, chlorite/smectite R0	Hydrothermal alteration	Dudoignon *et al.* (1997)
Corrensite, chlorite	Hydrothermal alteration	Bettison-Varga and Mackinnon (1997)

study of the clay assemblages crystallized during the cooling history of different types of basaltic bodies related to a single magmatic chamber. In the present study, three hawaiitic bodies (all with chilled margins and massive inner parts) from Mururoa Atoll (French Polynesia), which were selected far from hydrothermal zones and the present sea-water interface, were selected for investigation. In this study, close attention was focused on the clay mineralogy and, particularly, on both the crystal structure and compositional variation of the different types of clay minerals formed in the quenched and massive zones of these basalt-hawaiitic bodies. These mineralogical results will help to complete the overall petrographic and geochemical study dealt with in a related study (Meunier *et al.*, 2008).

GEOLOGICAL SETTINGS

The Mururoa Atoll (southeastern Tuamotu Archipelago, French Polynesia) belongs to the Pitcairn-Gambier Islands (Figure 1a,b), the formation of which is classically attributed to the activity of a hot spot (Thorpe and Smith, 1975). The $^{40}K/^{40}Ar$ age of the Mururoa Atoll is 10.3−11.8 Ma (Caroff, 1992).

The rocks studied here were sampled in the Fuschia drill-hole which is located outside the hydrothermal zones of the Mururoa Atoll (Figure 1c). From top to bottom, the sequence of rock units is coralline limestone, dolomites, volcano-sedimentary rocks, aerial, subaerial, and finally submarine flows (Bardintzeff *et al.*, 1986). Three basaltic bodies were selected: a submarine flow (basalt, 1.70 m thick, sampled between 697.60 and 695.90 m), a subaerial flow (hawaiite, 3.60 m thick, sampled between 644.10 and 640.70 m), and a dike (basalt, 1.60 m thick, sampled between 718.45 and 719.45 m). The base and top of the submarine and subaerial flows have 3−7 cm thick quenched margins. The upper one is brecciated. The inner massive parts are 1.60 m and 3.50 m thick, respectively, and highly crystalline. The dike also has quenched margins (3−7 cm thick) and a large, inner, massive part (1.50 m thick). The samples selected for the present study, together with their chemical compositions, are indicated in Tables 2 and 3. According to Maury *et al.*

Table 2. Location and macroscopic petrographic characteristics of the samples from the subaerial and submarine flows and from the dike (Mururoa Atoll, French Polynesia).

Volcanic body	Depth (m)	Petrographic characteristics
Subaerial (hawaiite, 3.60 m thick)	−640.70	Brecciated glass 3−5 cm thick
	−642.40	Gray aphyric massive rock
	−644.10	Massive glass 5−7 cm thick
Submarine (basalt, 1.70 m thick)	−695.90	Brecciated glass, 5 cm thick
	−697.00	Gray massive rock , olivine phenocrysts
	−697.60	Massive glass 5−7 cm thick
Dike (hawaiite, 1.60 m thick)	−718.45	Massive glass, 2−3 cm thick
	−719.45	Gray aphyric massive rock

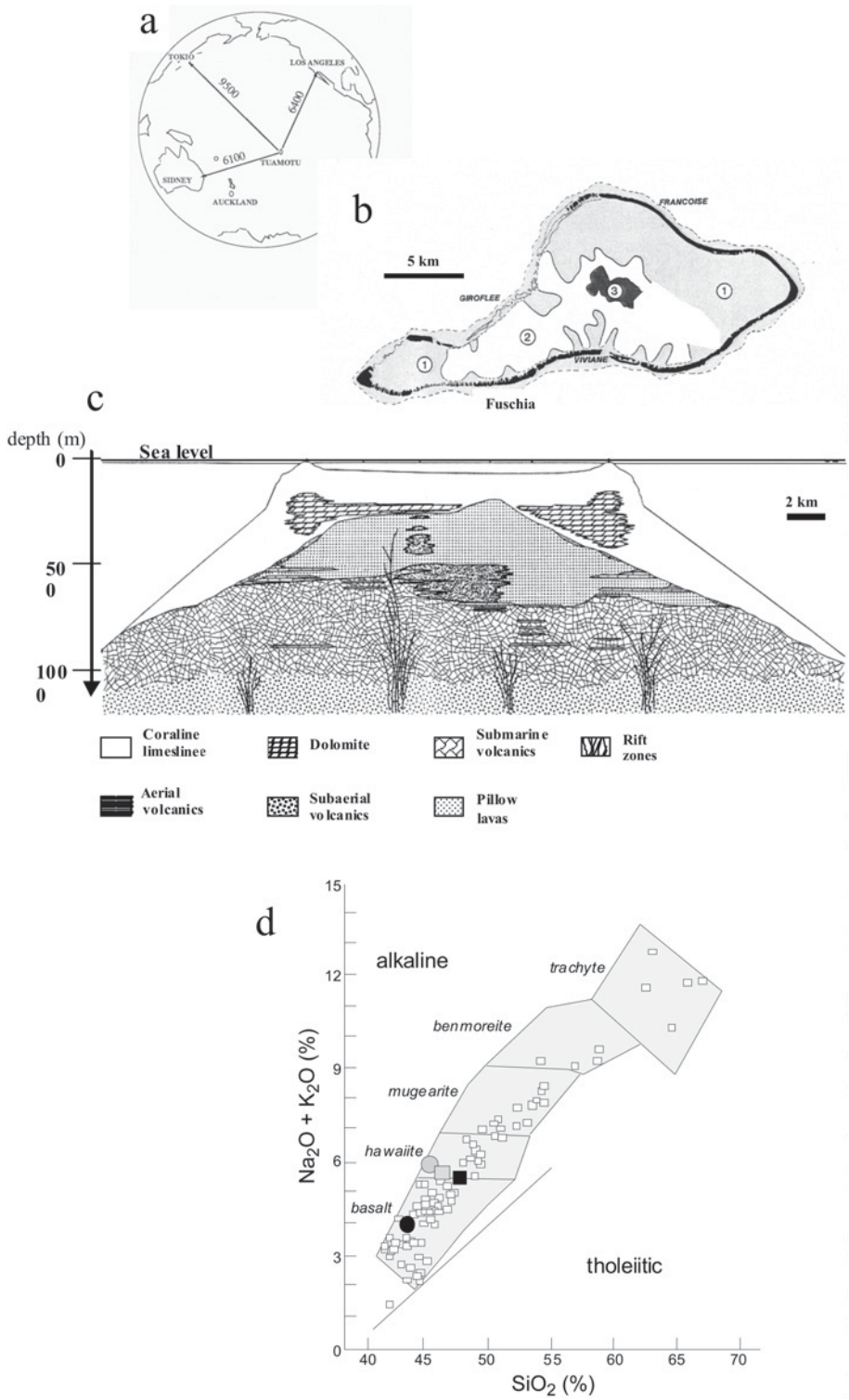

Figure 1. The Mururoa Atoll (French Polynesia). (a) Location of the Tuamotu Archipelago in the Pacific Ocean. (b) Location of the Fuschia drill hole on the reef barrier. (c) Schematic SW–NE cross-section of the geological structure showing the location of the Fuschia drill hole. The rift zones are strongly hydrothermalized. Arrows indicate the locations of the samples studied. sa: subaerial lava flow; sm: submarine lava flow; dy: dike. (d) Chemical composition of volcanic rocks from the magmatic series of Mururoa Atoll in the $Na_2O\% + K_2O\%$ *vs*. $SiO_2\%$ (Cox *et al.*, 1979): small squares – data from Maury *et al.* (1992); large square – subaerial flow; filled circle – submarine flow; circle – dike.

Table 3. Bulk-rock chemical composition (major elements).

	Subaerial			Submarine			Dike	
	chilled margin	massive inner part	brecciated	chilled margin	massive inner part	brecciated	chilled margin	massive inner part
Depth (m)	−644.1	−642.4	−640.7	−697.6	−697,00	−695.9	−718.45	−719.45
SiO_2	42.43	46.64	48.19	37.87	43.32	41.80	46.53	44.31
Al_2O_3	14.31	15.66	16.21	13.24	14.9	14.74	15.36	14.95
Fe_2O_3	11.72	12.61	10.79	14.73	13.39	12.12	10.03	13.11
TiO_2	4.80	3.56	3.28	5.50	4.56	4.46	3.32	3.88
MgO	6.19	4.40	3.80	6.51	4.83	5.77	2.05	3.71
MnO	0.09	0.19	0.15	0.19	0.21	0.12	0.19	0.12
CaO	5.10	8.53	8.58	5.38	10.31	4.43	6.11	7.48
Na_2O	2.64	3.64	3.63	2.81	2.30	4.14	5.14	3.48
K_2O	1.70	2.26	2.54	1.66	1.73	2.01	3.26	2.59
P_2O_5	0.76	1.04	0.96	0.75	0.55	0.31	0.85	0.69
LOI	10.23	1.87	2.30	11.84	3.90	10.02	7.15	5.69
Total	99.97	100.4	100.43	100.48	100,00	99.92	99.99	100.01

LOI: loss on ignition.
Total Fe is considered as Fe^{2+}.

(1992), the Mururoa volcanic flows belong to a classical alkali series in which hawaiites and basalts are the most common rock types while trachytes are rare. The series is characterized by large amounts of Fe. The compositions of the three volcanic bodies studied plot in the basalt-hawaiite domains (Figure 1d).

METHODS

Thin sections were prepared from samples of the quenched margins and of the massive parts of the three volcanic bodies. Petrographic observations were performed using a polarizing microscope. The proportions (vol.%) of phenocrysts, mesostasis, and glass were estimated from photomicrographs. Optical cathodoluminescence (CL) is a useful addition to the petrographic observations because CL enables plagioclase to be distinguished from K-feldspars (which appear as dark- and light-blue bodies, respectively) at thin-section scale. (The difference in luminescence is related to the presence of Ti^{4+} ions in K-feldspar; Marshall, 1988). Apatite crystals appear as bright red grains. Glass, pyroxene, olivine, Fe-Ti oxides, and clay minerals do not luminesce. Observations have been performed using a Technosyn 8200 Mark II-type stage associated with a high-tension generator and an Olympus BH2 optical microscope (vacuum condition: 5×10^{-2} Torr, 15−20 kV, 200−300 μA).

Each sample was ground in an agate mortar. The clay fraction (<2 μm) was extracted from suspensions in distilled water by centrifugation. The clays were analyzed in their natural state (no ionic saturation). X-ray diffraction (XRD) was performed from randomly oriented powders and oriented preparations in four different states: air-dried (AD), ethylene glycol solvated using a vapor phase at 60ºC (EG), heated to 300ºC (HAD), heated to 300ºC, and glycolated (HEG). The XRD patterns were recorded using a Philips PW 1730 diffractometer (CuKα radiation, 40 kV, 40 mA), equipped with a stepping motor drive (SOCABIM DACO system) and a keVEX solid-state detector. The analytical conditions were 2−35º2θ angular range, 0.025º2θ step size, 4 s counting time for oriented preparations; and 59−64º2θ angular range, 0.025º2θ step size, 8 s counting time for randomly oriented powders.

The XRD patterns from the oriented preparations were decomposed in the 2−10º2θ CuKα range, into Gaussian and Lorentzian elementary bands using the *DECOMPXR* program (Lanson 1997). The precision of the angular position is sometimes limited by the low intensity of the peak under consideration. This is the case for the 060 diffraction bands (only 2 significant decimals). When the positions of the elementary bands in the AD, EG, HAD, and HEG states converge to a single solution given by the *Newmod*© software (Reynolds, 1985), identification of the clay minerals is

considered reasonable. The results were deemed acceptable when the chemical composition (microprobe analyses), the position of the 060 diffraction bands, and the related infrared (IR) spectra concurred.

The IR spectra were recorded using a Nicolet 510 Fourier Transform Infrared (FTIR) spectrometer in transmission mode. The spectrometer was purged continuously with dry CO_2-depleted air. Pressed pellets (4 mg of sample mixed with 300 mg of KBr) were analyzed at a resolution of 4 cm^{-1} in the 4000−400 cm^{-1} range. Microanalyses were performed on thin sections using a CAMECA SX50 microprobe equipped with wavelength dispersive spectrometers. The analytical conditions were: 4−20 nA, 15 kV, spot size 10 μm, 100 s counting time, and beam intensity of 6×10^{-10} A. Quantitative analyses were obtained by comparison with natural silicate standards using a ZAF correction program. Because the Fe oxidation state was not measured, Fe was arbitrarily considered to be trivalent for smectites and divalent for chlorites. Because chemiographic analysis avoids the drawbacks of structural-formula calculation, in which errors arise due to the mixing or interstratification of 2:1 and 2:1:1 layer types (Meunier *et al.*, 1991), the M^+/4Si *vs.* Fe/sum octahedral (oct) cations plot was used. These coordinates permit representation of the solid-solution domains of di- and trioctahedral species (Meunier and El Albani, 2007). (1) The M^+/4Si ratio corresponds to the layer charge (Na +K + 2Ca) divided by the tetrahedral charge because 4Si = 1 or <1 for celadonite−montmorillonite or other phyllosilicates, respectively. (2) The total Fe content is divided by the sum of non-tetrahedral and non-interlayer cations, *i.e.* the sum of octahedral cations (Fe/sum oct). Because the number of octahedral cations depends on the basis used for the calculation of the unit formula (Beaufort and Meunier, 1994), errors in absolute values are unavoidable. This implies that relative proportions should be used instead of absolute values. The gray zones in Figure 2 represent the compositional domain of clay minerals commonly found in basaltic rocks: saponite − from a pure Mg end-member to the highest Fe-rich values (Desprairies *et al.*, 1989); chlorite − considering that the number of Al cations in octahedral sheets of the most common trioctahedral chlorites is roughly 1 per Si_4O_{10}, the theoretical composition field extends from pure Mg end-member (Fe/sum oct = 0) to the highest Fe-rich values (Fe/sum oct = 5/6); nontronite − from high- to low-charge, according to Koster *et al.* (1999); celadonite: theoretical composition as given by Odom (1984).

Most of the compositions of clay assemblages found in altered basaltic rocks plot in the Fe-rich saponite–chlorite–celadonite field. The Mg-rich clays plot in the chlorite−saponite field (Bettison and Schiffman, 1988; Bettison-Varga and Mackinnon, 1997; Schiffman and Fridleifson, 1991; Schmidt and Robinson, 1997; Neuhoff *et al.*, 1999). Microprobe analyses are presented here as plots in M^+/4Si *vs.* Fe/sum oct diagrams only.

RESULTS

Clay minerals from altered glass in the quenched margins

Subaerial flow. The quenched margin at the base of the flow (−644.10 m) is composed of a brown glass matrix (45%) in which are scattered numerous plagioclase microliths (10−70 μm long, ~26%), pyroxene and Ti-Fe oxide microcrysts (1−2% and 3−4%, respectively), and scarce olivine microcrysts (Figure 3a). Cathodoluminescence reveals that the plagioclase microliths are unaltered (Figure 4a). This is confirmed by random powder XRD which confirms the absence of albite. Numerous small apatite crystals are scattered in the glassy matrix (red grains in CL). The quenched margin is crosscut by veinlets 50−400 μm wide. Each exhibits a thin, green clay rim on the wallrocks (10 μm thick) and a central zeolite deposit (analcime +

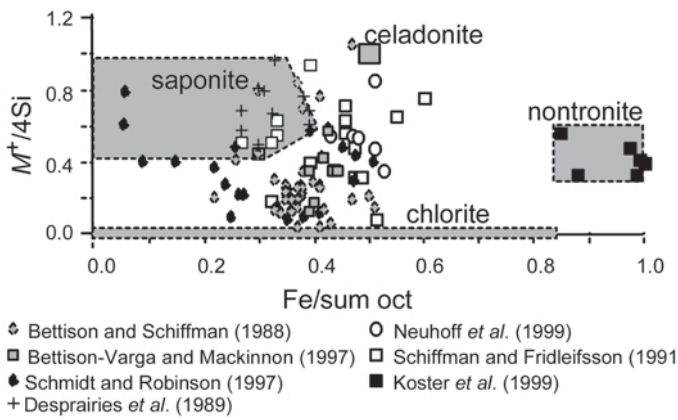

Figure 2. Compositions of the principal clay mineral species in the M^+/4Si *vs.* Fe/sum octahedral cations (Fe/sum oct). See text for details.*

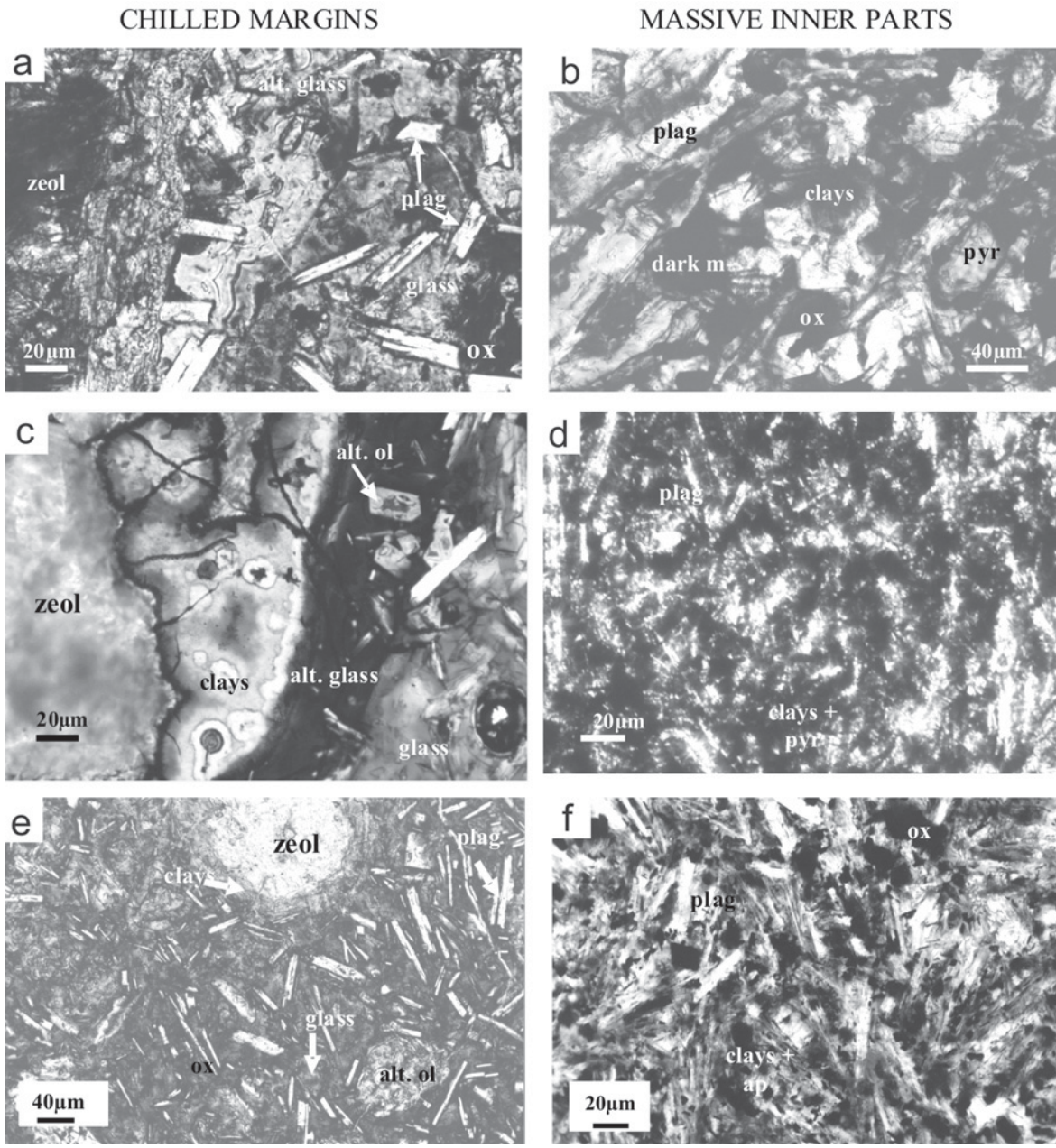

Figure 3. Photomicrographs of the chilled margins and massive inner parts of the subaerial (a–b) and submarine flows (c–d) and the dike (e–f). alt. glass: altered glass (palagonite-type); glass: unaltered basaltic-hawaiite glass; plag: plagioclase; ox: Fe oxides; pyr: pyroxene; alt. ol: altered olivine; zeol: zeolite; dark m: dark mesostasis (Fe-Ti oxide + pyroxene + plagioclase); ap: apatite.

phillipsite). The glass in contact with the veins is altered (palagonite-like, 10–100 µm thick). The upper quenched margin (–640.70 m) is brecciated. The volcanic rock pieces in the breccia are coated by the same green clay deposit and cemented by zeolites (analcime + phillipsite).

The position of the 001 diffraction band shifts from 14–15 Å (AD) to 16.9–17.1 Å (EG) indicating that the clay minerals are essentially composed of smectites. This is consistent with the relatively intense 002 diffraction peak at 8.5 Å in the EG state (Figure 5a). The microanalyses (Figure 6) confirm a polyphase assemblage consisting of a trioctahedral smectite (saponite) and a dioctahedral Fe-rich smectite. This is consistent with the presence of two 060 diffraction bands at 1.53 and 1.52 Å. The IR absorption bands at 3570, 817 (Fe^{3+}-Fe^{3+}-OH), and 875 cm^{-1} (Al-Fe^{3+}-OH) are typical of a nontronite, while that at 3625 (2Mg-Fe^{3+}-OH) and 675 cm^{-1} (3Mg-

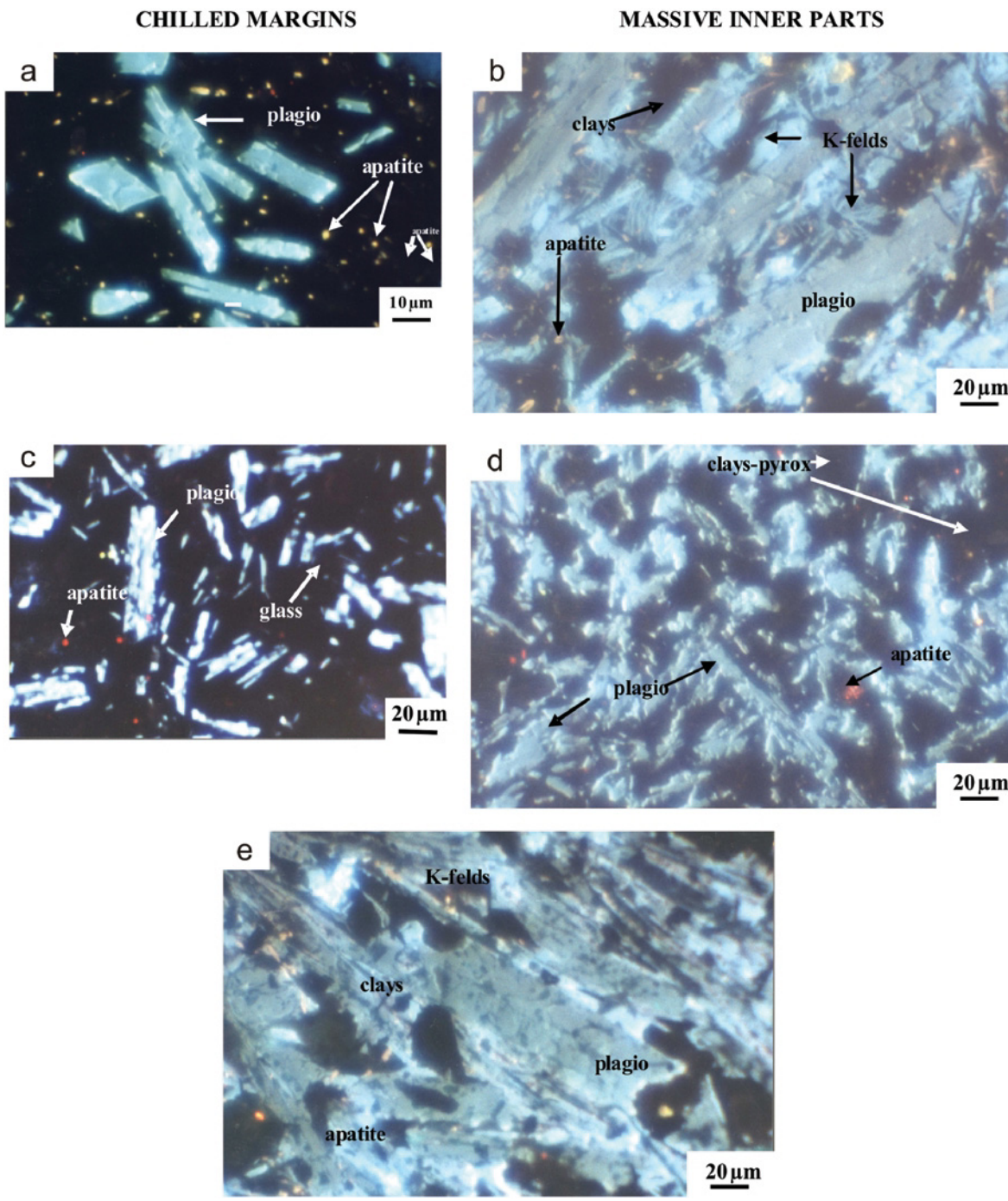

Figure 4. Cathodoluminescence images of the chilled margins and massive inner parts of the subaerial (a–b) and submarine flows (c–d) and the massive part of the dike (e). Light blue: K-feldspar overgrowths; dark blue: plagioclase microliths; black areas: glass, clay mesostasis, or Fe-Mg bearing crystals (pyroxene, olivine); red-yellow: apatite crystals.

OH) are typical of a trioctahedral phase (saponite) (Figure 5b). Using the M^{+}/4Si *vs.* Fe/sum oct coordinates, the microanalyses plot in the Fe-saponite–chlorite–nontronite–celadonite field (Figure 6). With each plot representing a mixture of Fe-saponite and a dioctahedral Fe-rich smectite, the compositional domain indicates that the dioctahedral Fe-rich smectite component is significantly different from typical nontronites because of the greater Al content and unusually high layer charge. The heating treatments (HAD and HEG) outline the layer charge heterogeneity; the high-charge layers remain collapsed at ~10 Å after ethylene glycol solvation.

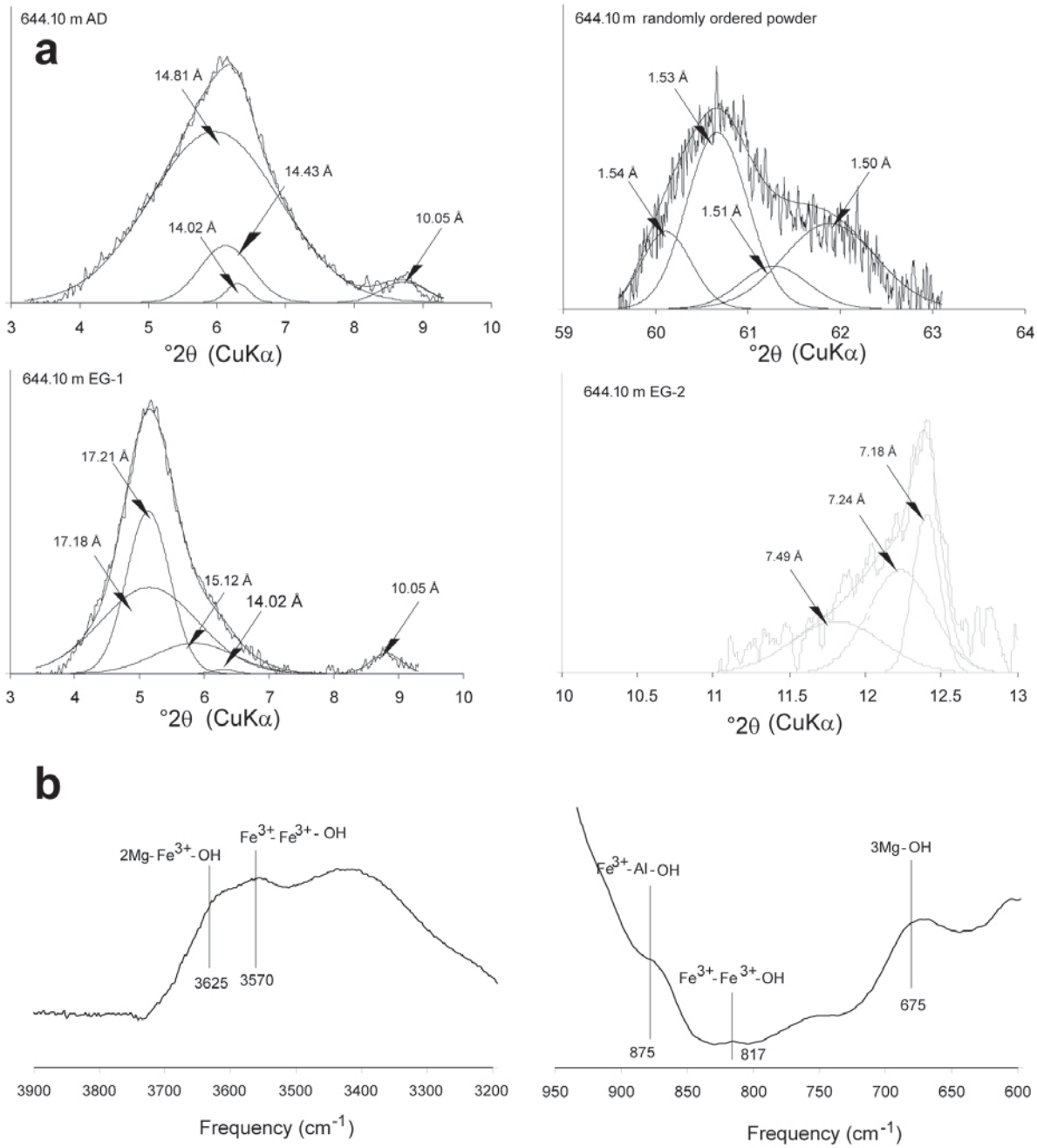

Figure 5. Chilled margin of the subaerial flow (−644.10 m; hawaiite). (a) XRD patterns of the <2 μm fraction. AD: air-dried; randomly ordered powder: 060 diffraction bands; EG-1 and EG-2: ethylene glycol solvated (2−10 and 8−14º2θ CuKα, respectively); HAD: heated to 300ºC; HEG: heated to 300ºC and ethylene glycol solvated. (b) IR absorption spectra in the 3900−3200 and 950−600 cm^{-1} wavelength ranges.

Submarine flow. The chilled margin (−697.60 m) is composed of a glassy matrix (~45%) with numerous disseminated plagioclase microliths (10 and 80 μm long; ~26%), Ti-Fe oxide microcrysts (~3%), and clay pseudomorphs of a few olivine microcrystals (Figure 3c). Vesicles (~19%) and veins (~16%) are filled by green clay minerals and zeolites (analcime + phillipsite). The vesicle and vein wallrocks are rimmed by a brown palagonite-like material contrasting with the orange, unaltered glass. The plagioclase microcrysts are not altered (Figure 4c). Apatite microcrystals are scattered in the glass. The upper quenched margin (−640.70 m) is a breccia in which the volcanic rock pieces are coated by a green to colorless clay deposit and cemented by zeolites (analcime + phillipsite).

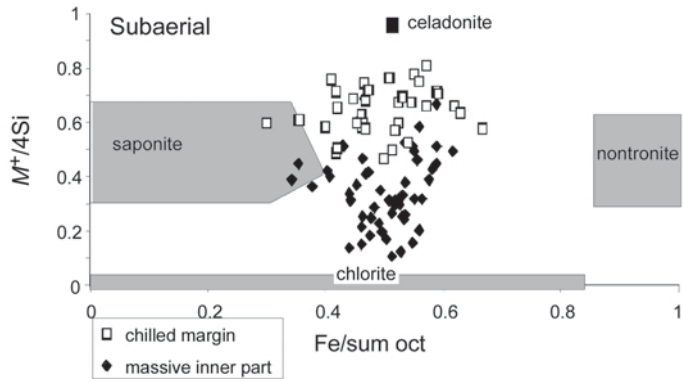

Figure 6. Subaerial flow. The chemical composition of the clay mineral assemblages (microprobe analyses) are plotted in the M^+/4Si *vs.* Fe/sum oct coordinates (see text for details).

Decomposition of the XRD patterns of the clay fraction (Figure 7a) revealed a shift in positions of the 001 diffraction bands in the air-dried and ethylene-glycol solvated states, indicating the presence of expandable and non-expandable minerals. The XRD pattern of the non-expandable phase is typical of a chlorite-like structure: the 001 and 002 diffraction bands at 14.02 and 7.20 Å are identifiable both in the AD and EG patterns. The sharp 7.20 Å and broad 7.60 Å bands are assigned to chlorite with a large coherent-scattering domain size and mixed-layer chlorite smectite, respectively. The XRD reflections of expandable phases are complex because they do not fully expand to 17 Å. The 001 positions at 16 and 16.7 Å indicate the presence of at least two randomly ordered mixed-layer smectite-chlorites (MLMs), the composition of which can be approximated using NEWMOD simulations:

MLM1 (15.98 Å and 7.60 Å):
DiSm Fe = 1.7 (55%) – Tri-Trichl Fe = 1 (45%)
MLM2 (16.66 Å and 8.40 Å):
TriSm Fe = 0.33 (80%) – Tri-Trichl Fe = 1 (20%)

This is consistent with the XRD pattern of the 300ºC heated sample: the peaks at 12.48 Å and 10.08 Å correspond to MLM1 and MLM2, respectively. The ethylene glycol solvation of the heated sample shows that only some of the smectite layers re-expand. Some layers remain collapsed at 10 Å, indicating that the layer charge is sufficient to fix the K ions present in the interlayer region irreversibly.

The broad diffraction band in the 59–64º2θ CuKα angular range results from the summation of three 060 peaks: 1.52 Å from Fe-rich dioctahedral layers (nontronite-type); 1.53 Å from Mg-rich trioctahedral layers (saponite-type); and 1.54 Å from tri-tri chlorite. The coexistence of Fe- and Mg-rich phases is supported by the IR absorption bands at 3571, 875, 650, and 506 cm^{-1} which are typical of the Fe^{3+}-Fe^{3+}-OH, Fe^{3+}-Al-OH, 3Mg-OH, and Si-O-Fe^{3+} groups, respectively (Figure 7b), and the chemical compositions of the clay assemblages which plot between the celadonite and Fe-saponite end-members in the M^+/4Si *vs.* Fe/sum oct coordinates (Figure 8). In summary, the clay fraction of the chilled margins from the submarine hawaiite flow is composed of two randomly mixed-layer minerals (saponite-chlorite and nontronite-chlorite types) and chlorite.

Dike. The chilled margin (–718.45 m) is 2–3 cm thick. It consists of a yellow glassy matrix containing numerous plagioclase microliths and Ti-Fe oxide microcrysts (Figure 3c). Olivine microcrysts are rare and pseudomorphosed systematically by clay minerals. Veinlets (10–30 μm wide) and micro-vesicles are filled by green clay minerals. The volcanic glass of the wallrocks is altered (palagonite-like). Colorless clays and zeolites (analcime + phillipsite) fill the vein and vesicle center.

The clay fraction is composed of expandable and non-expandable clay minerals (Figure 9a). Decomposition of the XRD pattern of the glycolated sample shows that the expandable minerals are randomly ordered mixed layers consisting of fully (2 EG) and partly (1 EG) expandable layers. A *Newmod* simulation indicates a composition as follows:

d_{001} = 16.78 Å: DiSm 2Gl (95%) – DiSm 1Gl (5%)
d_{001} = 13.79 Å: DiSm 1Gl (75%) – DiSm 2Gl (25%)

The presence of non-expandable minerals is proven in the XRD patterns of the 300ºC-heated samples. The shift in position between the AD and EG states is very limited for the 10–10.07 Å and 11.47–11.26 Å diffraction bands. These bands can be attributed to celadonite and an ordered celadonite70%/chlorite30% MLM, respectively. The MLMs may have a small number of expandable layers.

In spite of the lack of an identifiable 060 peak (no significant diffraction was obtained in the 59–64º2θ CuKα range), the presence of Fe-rich dioctahedral and Mg-rich trioctahedral phyllosilicates is confirmed by the Fe^{3+}-Al-OH and Fe^{3+}-Fe^{3+}-OH IR absorption bands at 875 and 822 cm^{-1}, respectively. In the present case, the 3Mg-OH absorption band at 670 cm^{-1} is due to the

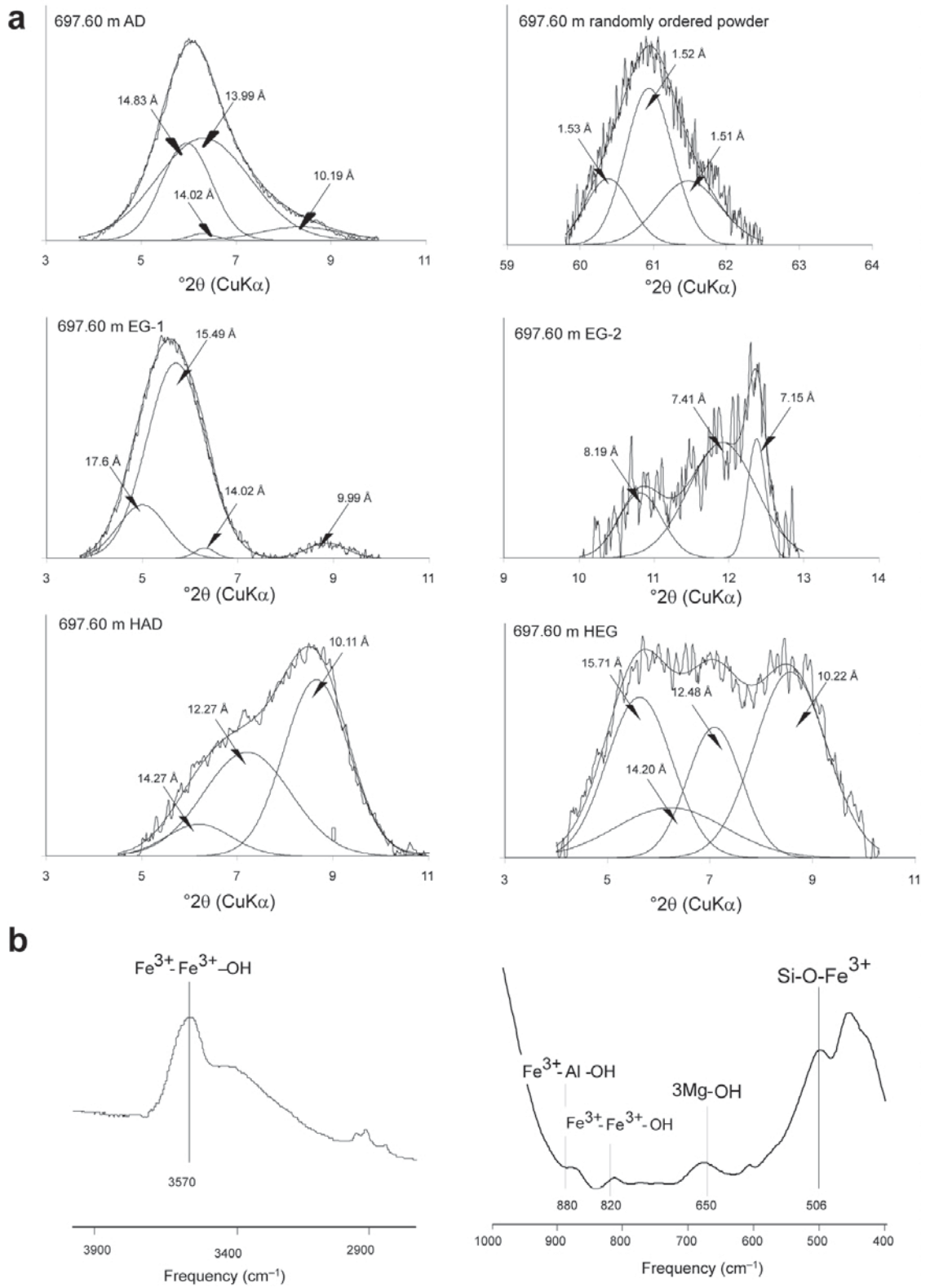

Figure 7. Chilled margin of the submarine flow (−697.60 m; basalt). (a) XRD patterns of the <2 μm fraction. AD: air-dried; randomly ordered powder: 060 diffraction bands; EG-1 and EG-2: ethylene glycol solvated (3−9 and 8−15º2θ CuKα, respectively); HAD: heated to 300ºC; HEG: heated to 300ºC and ethylene glycol solvated. (b) IR absorption spectra in the 3900−2900 and 1400−400 cm^{-1} wavelength ranges.

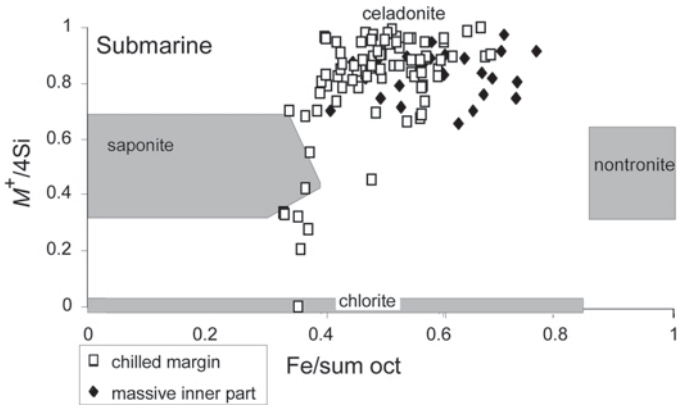

Figure 8. Submarine flow. The chemical composition of the clay mineral assemblages (microprobe analyses) are plotted in the M^+/4Si *vs.* Fe/sum oct coordinates (see text for details).

presence of chlorite layers (Figure 9b), consistent with the chemical compositions which plot in a large area between the celadonite, nontronite, and chlorite poles in the M^+/4Si *vs.* Fe/sum oct coordinates (Figure 10).

Clay minerals in the microvesicles and mesostasis

Massive part of the subaerial flow. The massive, inner part of the subaerial flow (hawaiite) does not contain any vesicles or veinlets (Figure 3d). It is highly crystalline and consists of pyroxene microcrysts (10−60 μm, ~8%), plagioclase pheno- and microcrysts (80 μm−4 mm, ~49%), and Fe-Ti oxide microcrysts (~11%). The mesostasis consists of green clayey patches (10−80 μm wide, ~20%) or dark gray/black microzones (~12%) in which Fe-Ti oxides are concentrated. K-feldspar is observed as discrete microcrysts in the mesostasis or as overgrowths on plagioclase microcrysts. Apatite microcrysts (red grains) are scattered in the clay matrix (Figure 4b).

Figure 11a shows that the clay fraction in the green mesostasis comprises expandable and non-expandable minerals: chlorite (14.02 and 7.18 Å) − the 7.24 Å diffraction band is probably due to chlorite particles with small coherent-scattering domain size, and mica (10.05 Å); smectite (14.81 Å AD and 17.21-17.16 Å EG); and a randomly ordered MLM chlorite/smectite (14.48 Å, 16.12 Å and 7.49 Å). The composition of the chlorite-smectite MLMs is approached using *Newmod* calculations for the 16.12 Å and 7.49 Å diffraction peaks: randomly ordered Tri-Trichl Fe = 1 (65%)−TriSm Fe = 0.33 (35%).

No significant diffraction patterns were obtained after heating to 300ºC. The mica phase is of celadonite type (d_{060} = 1.51 Å). The smectite and chlorite-MLM phases are trioctahedral: d_{060} at 1.53 Å and 1.54 Å, respectively. The presence of the celadonite-type phase is confirmed by the IR absorption bands at 3570 and 3.575 cm^{-1}, typical of the Fe^{3+}-Fe^{3+}-OH and Fe^{2+}-Al-OH bonds, respectively (Figure 11b). The presence of trioctahedral groups (3Mg-OH) is proven by the 675 cm^{-1} absorption band. The Mg-rich phases are dominant, as shown by their composition domain in the M^+/4Si *vs.* Fe/sum oct coordinates (Figure 6).

Massive part of the submarine flow. The crystalline matrix of the basaltic rock consists of phenocrysts and microphenocrysts of olivine (2−150 μm; ~7%), pyroxene (10 μm−5 mm; ~9%), plagioclase (10 μm−3 mm; ~37%), and Fe-Ti oxides (2−50 μm ~12%). The cryptocrystalline mesostasis presents two different forms (Figure 3e): green to brown patches (10−100 μm; ~22%) consisting of clay minerals and dark gray/black zones (10−100 μm; ~13%) rich in Fe-Ti oxide microcrysts. The olivine phenocrysts and microphenocrysts are pseudomorphically replaced by green clay minerals. Some veinlets (1−2 mm wide) crosscut the basalt. They are rimmed by clay deposits and sealed by zeolites (analcime + phillipsite). Numerous microvesicles (60−400 μm in diameter) are scattered in the basalt and filled by green clay minerals; the largest (>100 μm) exhibit a zoned mineral deposit: green clay minerals in the outer rim, colorless ones in the center. The microvesicles are sometimes connected with the green mesostasis. No K-feldspar overgrowths were observed on the plagioclase microcrysts. Apatite microcrystals are scattered in the mesostasis (Figure 4d).

Figure 12a shows that the clay fraction extracted from the microvesicles and the mesostasis voids consists of expandable and non-expandable minerals. The latter are mainly chlorite (14.02 Å and 7.16 Å). The expandable minerals are characterized by the shift of the 13.99 and 14.83 Å bands (AD) to 17.66 and 16.49 Å after glycolation. Two randomly ordered chlorite/smectite MLMs were identified using *Newmod:* MLM1 (16.5 Å and 8.19 Å): TriSm Fe = 0.33 (70%) − Tri-Trichl Fe = 1 (30%); MLM2 (7.41 Å): DiSm Fe = 1.7 (30%) − Tri-Trichl Fe = 1 (70%).

After heat treatment at 300ºC, the 001 diffraction peaks shift to 12.27 Å and 10.11 Å. These positions correspond to MLM2 and MLM1, respectively. The

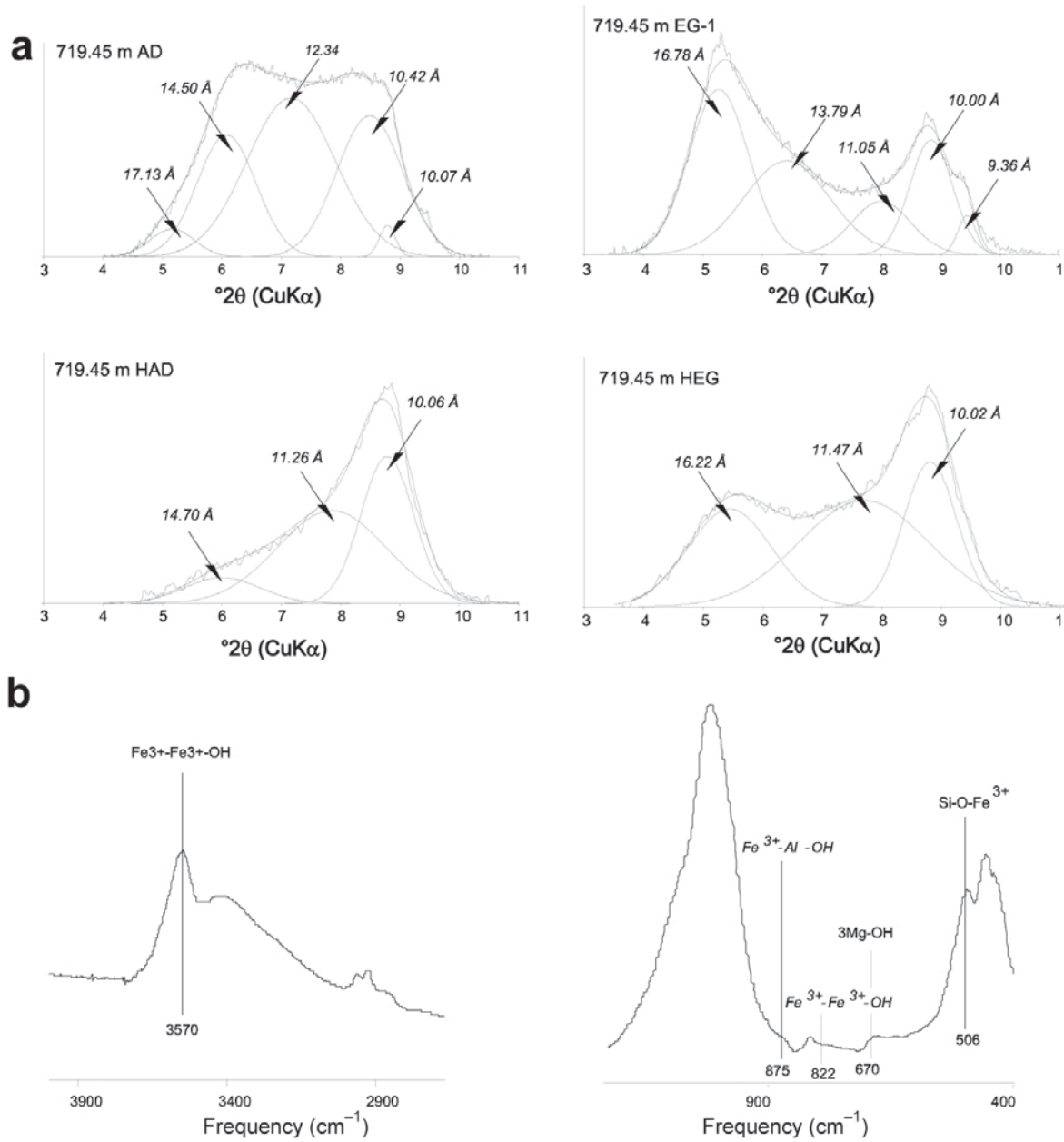

Figure 9. Chilled margin of the dike (−719.45 m; hawaiite). (a) XRD patterns of the <2 μm fraction. AD: air-dried; EG-1 ethylene glycol solvated (3−11°2θ CuKα); HAD: heated to 300ºC; HEG: heated to 300ºC and ethylene glycol solvated. (b) IR absorption spectra in the 3900−2900 and 1200−400 cm^{-1} wavelength ranges.

glycolation shows that not all of the smectite layers re-expand. Some remain collapsed at 10 Å, indicating the presence of high-charge layers in which K ions are irreversibly fixed. The 060 peaks at 1.53, 1.52, and 1.51 Å indicate the presence of trioctahedral and Fe-rich dioctahedral phyllosilicates, respectively. The IR absorption bands at 3570, 820 cm^{-1}, and 880 cm^{-1} (Figure 12b) are typical of the Fe^{3+}-Fe^{3+}-OH and Fe^{3+}-Al-OH bonds (high-charge Fe-rich smectite). The 650 cm^{-1} absorption band (3Mg-OH) confirms the presence of a trioctahedral structure (chlorite/smectite MLMs). The expandable component of all the clay phases is an Fe-rich and probably high-charge smectite. This is confirmed by the chemical analyses of the clay fraction which plot in the vicinity of the celadonite end-member in the M^{+}/4Si *vs.* Fe/sum oct coordinates (Figure 8).

Massive part of the dike. The hawaiite crystalline matrix (Figures 3f, 4e) consists of different microcryst species:

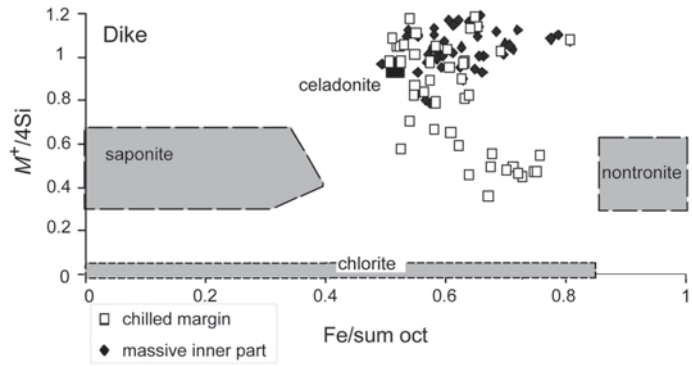

Figure 10. Dike. The chemical composition of the clay mineral assemblages (microprobe analyses) are plotted in the M^+/4Si *vs.* Fe/sum oct coordinates (see text for details).

pyroxene (10−40 μm, ~4%), plagioclase (20−200 μm, ~43%), and Ti-Fe oxide (14%). The gray microcrystalline mesostasis occupies 10% of the intergranular spaces. It appears as green-beige clays (24%). Vesicles (300 μm−4 mm in diameter) are disseminated into the crystalline matrix (5%). They are cemented by zeolite (analcime + phillipsite). K-feldspar and apatite microcrysts are scattered in the mesostasis (Figure 4e).

The green-beige clays are composed of expandable and non-expandable clay species (Figure 13a). The non-expandable phase is mainly of celadonite type as indicated by the 10.00−10.12 Å diffraction peak which is systematically present whatever the treatment, and by the d_{060} at 1.51 Å. The expandable phases are characterized by the shift in the diffraction bands from 10.85 and 14.12 Å (AD) to 11.20, 14.40, and 17.00 Å (EG). Moreover, the general collapsing to 10.66 and 10.04 Å after heating to 300ºC indicates that all these diffraction bands must be attributed to expandable phases. However, the partial re-expansion after glycolation of the heated sample indicates that the layer charge is variable: some of the expandable layers are high-charge and these remain collapsed at 10 Å.

The more intense 060 peak is that at 1.52 Å, indicating that the smectites are mainly of nontronite type. The trioctahedral smectite (saponite type; d_{060} = 1.53 Å) is less abundant and/or less crystalline. The presence of two smectite species is confirmed by the IR absorption bands at 3625 and 816 cm^{-1} (Fe^{3+}-Fe^{3+}-OH bonds), 875 cm^{-1} (Fe^{3+}-Al-OH bonds), and 675 cm^{-1} (3Mg-OH bonds) (Figure 13b). No chlorite phase was detected.

Because of the predominance of the Fe-rich phases, the smectite high-charge layers likely belong to nontronite- rather than to the saponite-type. If so, the 17.00 Å peak should correspond to the saponite-type (2 EG layers) while the 14.40 Å and 11.20 Å peaks would be attributed to a randomly ordered interstratification of 2EG-1EG nontronite-type layers. Because Fe-rich clay species are dominant, the 002 diffraction peaks are absent or broad and weak. Considering that the expandability depends on the layer charge, the amounts of Fe in the fully and partially expandable smectite layers have been fixed in the *Newmod* calculation to 1.7 and 1.4, respectively. An approximate composition of the MLMs has been calculated:

d_{001} = 14.40 Å: DiSm 1Gl (65%) − DiSm 2Gl (35%)
d_{001} = 11.20 Å: DiMica Fe = 1 (67%) − DiSm 1Gl (33%).

The predominance of the Fe-rich phases is consistent with the chemical composition of the green clays which plots near the celadonite−nontronite join in the M^+/4Si *vs.* Fe/sum oct coordinates (Figure 10).

DISCUSSION

Chemical and mineralogical compositions of the clay assemblages

The mineralogical composition of the clay assemblages in the quenched and massive inner parts of the three basaltic bodies is summarized in Table 4. All assemblages are composed of di- and trioctahedral phases encompassing expandable (nontronite, saponite types) and non-expandable layers (chlorite, celadonite types). These phases may be composed either of one layer type (mineral species) or two layer types (mixed-layer minerals). Both the mixture of different mineral phases and interstratification of different layer types induce the scattering of the chemical compositions measured by microprobe analysis between the Fe-saponite, chlorite, nontronite, and celadonite end-members in the M^+/4Si *vs.* Fe/sum oct coordinates (Figures 6, 8, 10). This is also the case for most of the clay assemblage compositions from low-grade metamorphic series or hydrothermal systems in spite of the fact that nontronite has not been identified (Figure 2). In that case, Fe is considered to be partitioned between the solid solutions of the trioctahedral phases (chlorite and saponite) because celadonite, when present, is supposed to be inherited from earlier alteration events. In such conditions, the X_{MgO} variation in chlorites was shown to be thermally controlled (Schiffman and Fridleifson, 1991; Schmidt and Robinson, 1997). However, because

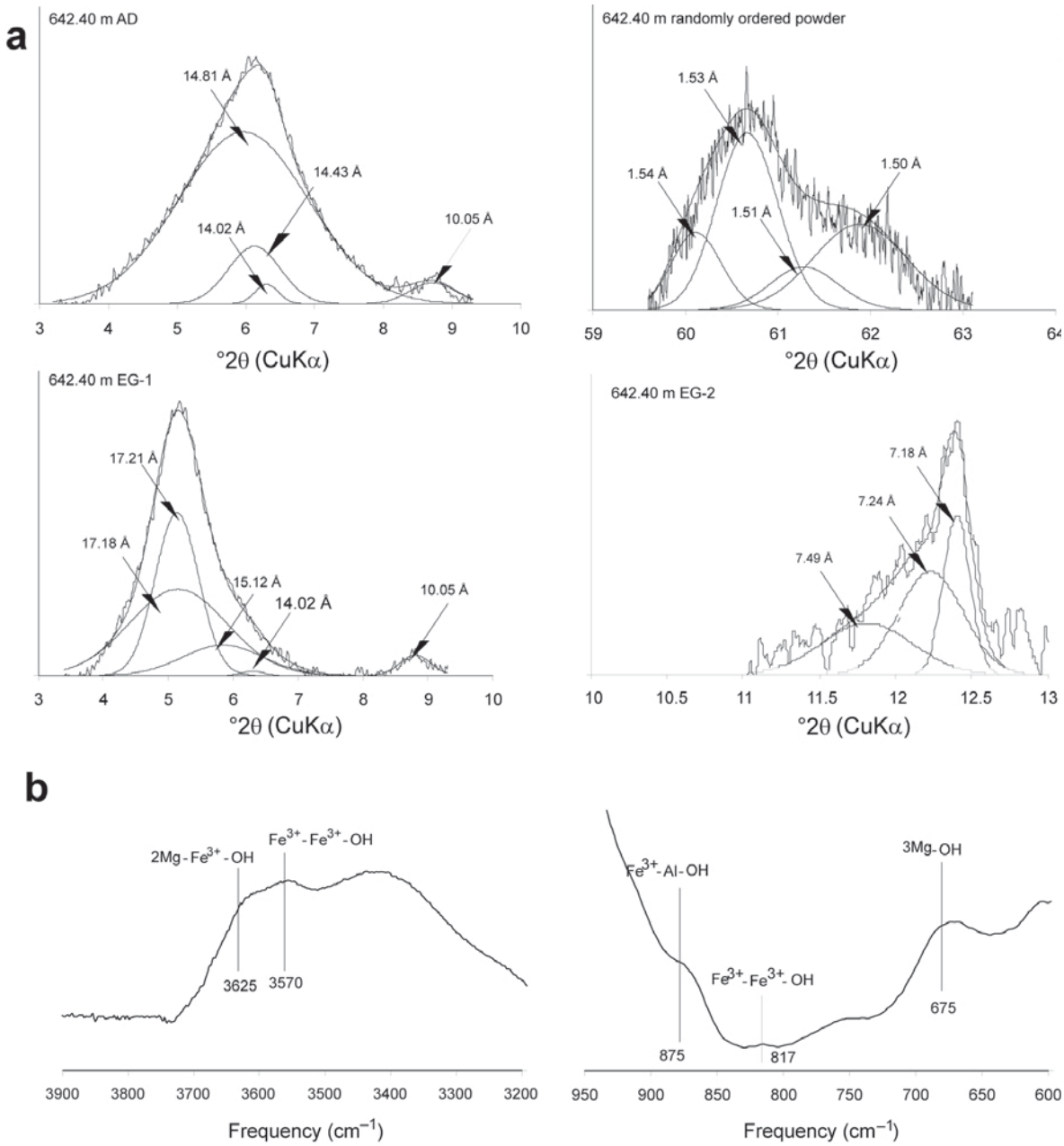

Figure 11. Massive inner part of the subaerial flow (−642.40 m; hawaiite). (a) XRD patterns of the <2 μm fraction. AD: air-dried; randomly ordered powder: 060 diffraction bands; EG-1 and EG-2: ethylene glycol solvated (3−10 and 10−13°2θ CuKα, respectively). (b) IR absorption spectra in the 3900−3200 and 950−800 cm^{-1} wavelength ranges.

of the systematic presence of coexisting Fe-rich phases in the Mururoa basalt-hawaiite system, the X_{MgO} values cannot be used as a geothermometer.

The chemical compositions of clay assemblages in the quenched margins and the massive inner crystallized parts of the three basaltic bodies studied here are not scattered in the same area of the Fe-saponite–chlorite–nontronite–celadonite field. First, the compositional fields of the clays from the quenched margins of the three volcanic bodies are similar; the clay material is richer in celadonite and di- or trioctahedral smectites than in chlorite. Consequently, the crystal-chemical properties of the clays in the quenched margins do not depend on the basalt-hawaiite glass composition but seem to be controlled by a strong water-rock interaction process which obliterated both the chemical and textural differences between the three volcanic bodies. This is typically the case when hydrothermal alteration is controlled by the continuous renewal of external solutions. On the contrary, the compositional fields of

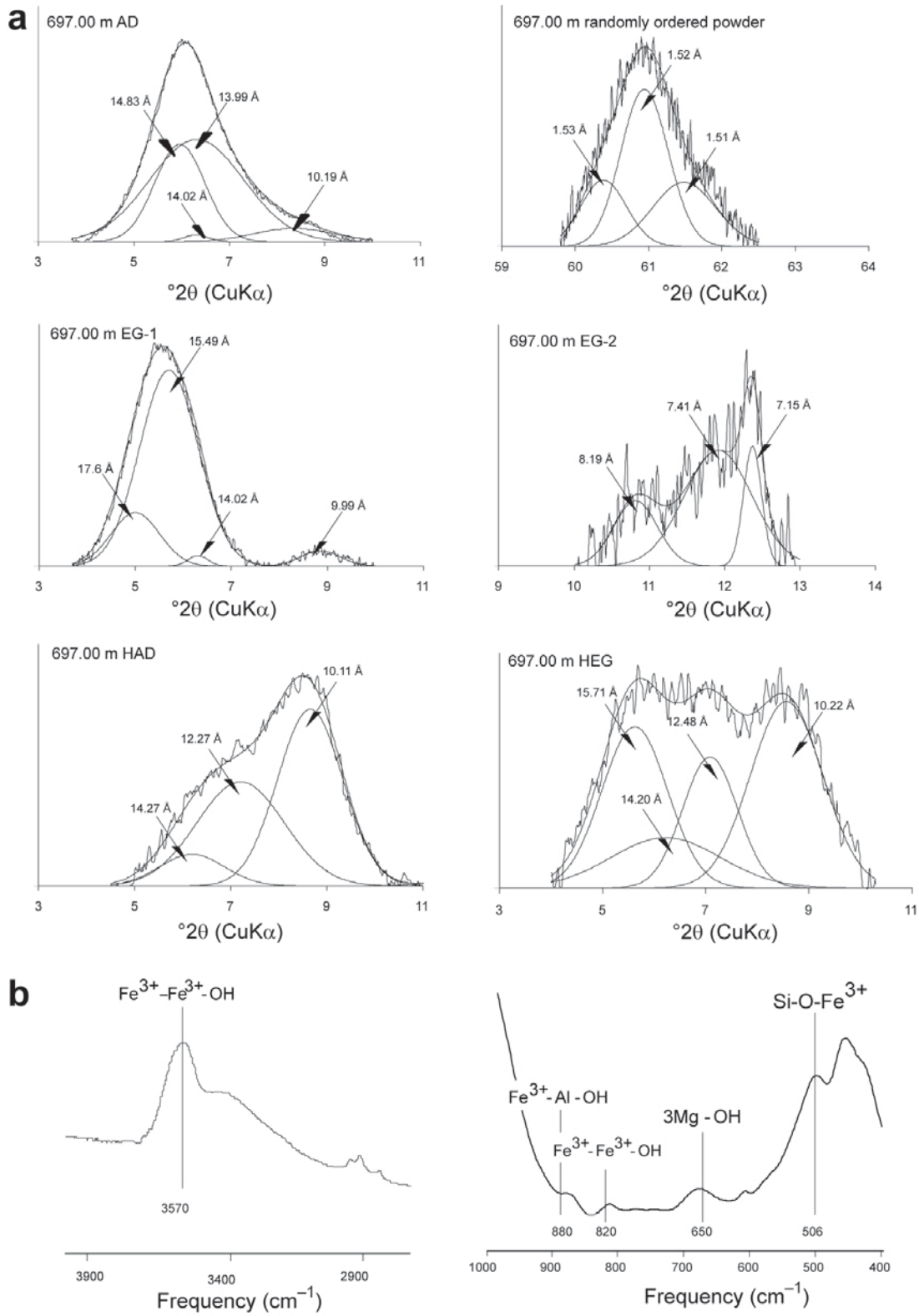

Figure 12. Massive inner part of the submarine flow (−697.00 m; basalt). (a) XRD patterns of the <2 μm fraction. AD: air-dried; randomly ordered powder: 060 diffraction bands; EG-1 and EG-2: ethylene glycol solvated (3−11 and 9−14°2θ CuKα, respectively); HAD: heated to 300°C; HEG: heated to 300°C and ethylene glycol solvated. (b) IR absorption spectra in the 3900−2900 and 1000−400 cm^{-1} wavelength ranges.

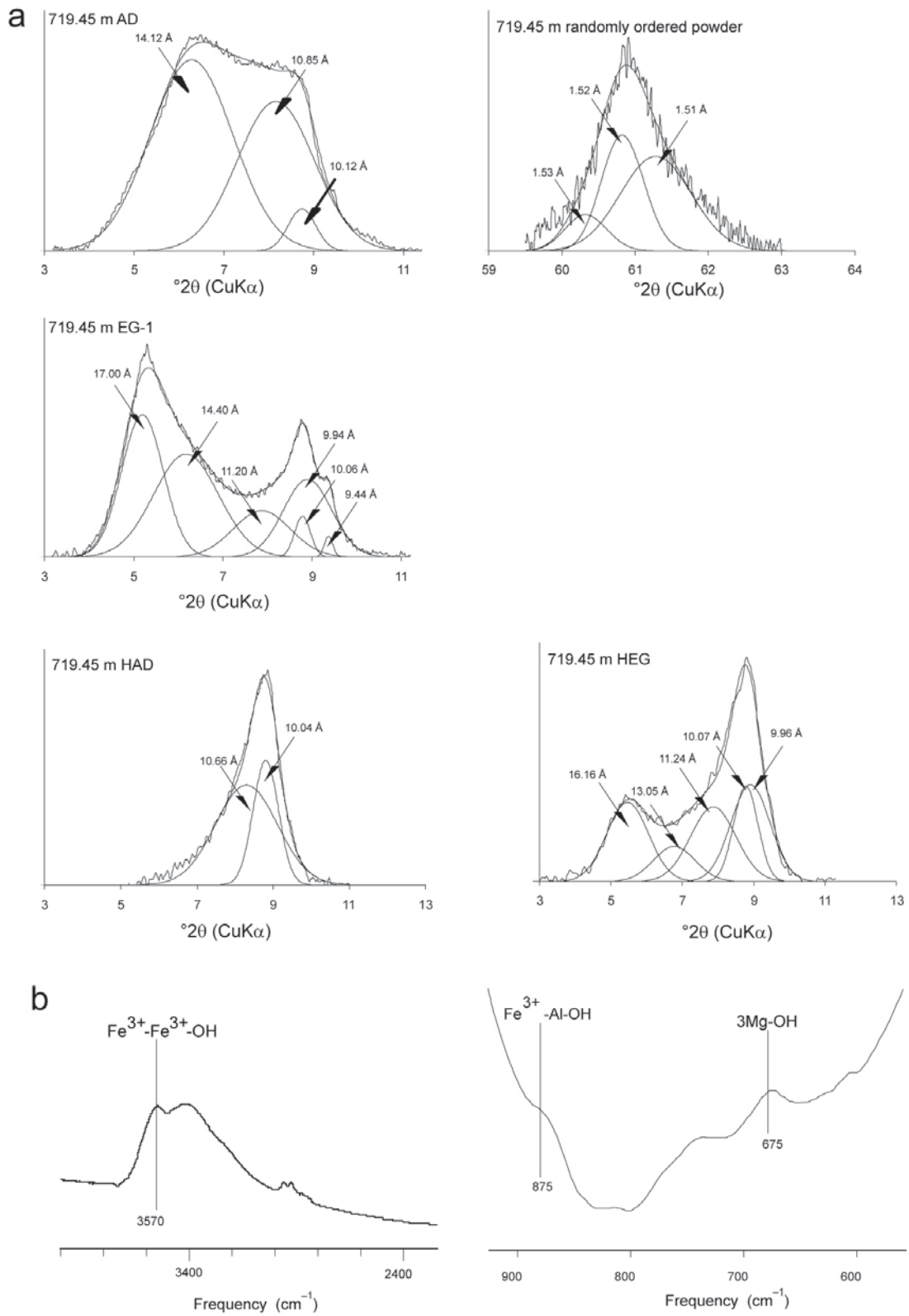

Figure 13. Massive inner part of the dike (−718.45 m; hawaiite). (a) XRD patterns of the <2 μm fraction. AD: air-dried; randomly ordered powder: 060 diffraction bands; EG-1 ethylene glycol solvated (3−11°2θ CuKα); HAD: heated to 300ºC; HEG: heated to 300ºC and ethylene glycol solvated. (b) IR absorption spectra in the 4000−2400 and 900−600 cm^{-1} wavelength ranges.

Table 4. Mineralogical composition of the vesicles, veins, and mesostasis deposits in the quenched margins and the massive inner parts of the subaerial and submarine flows and the dike (Mururoa Atoll, French Polynesia).

Volcanic body	Chilled margins (vesicles and veins)		Massive parts	
			Vesicles and veins	Mesostasis
Sub-aerial hawaiite	Analcime Phillipsite	Saponite Nontronite	No vesicles No veins	K-feldspar Apatite Saponite Sap_{35}/Chl_{65} MLM Celadonite
Submarine basalt	Analcime Phillipsite	Sap_{80}/Chl_{20} MLM No_{55}/Chl_{45} MLM Chlorite	Analcime Phillipsite Clay minerals	Pyroxene Apatite Sap_{70}/Chl_{30} MLM No_{30}/Chl_{70} MLM Celadonite
Dike hawaiite	Analcime Phillipsite	Nontronite Celadonite Cel_{70}/Chl_{30} MLM	Analcime Phillipsite Clay minerals	K-feldspar Apatite Nontronite Ce_{67}/No_{33} MLM Saponite

mesostasis clays in the massive inner part of the three basaltic bodies are not identical: they are chlorite-rich in the subaerial flow and celadonite- or high-charge nontronite-rich in the submarine flow and in the dike. Even if the compositional fields are partially superimposed (submarine flow and dike), the compositional variations could indicate that mesostasis clays do not crystallize from the same alteration process of basaltic glass as clays formed in the quenched margins.

Compared to the trioctahedral phyllosilicate sequence commonly described in hydrothermal systems (Bettison-Varga and Mackinnon, 1997; Dudoignon *et al.*, 1997; Schiffman and Fridleifsson, 1991) or low-grade metamorphism conditions (Schmidt & Robinson, 1997; Bevins *et al.*, 1991; Schiffman and Day, 1999; Neuhoff *et al.*, 1999), the clay assemblages of the three basaltic bodies studied here differ in the following manner: (1) in the absence of mineralogical variation between mesostasis and vesicles; (2) in the absence of corrensite; and (3) in the presence of nontronite-type clays. In low-grade metamorphism conditions, the smectite or smectite-rich C-S MLMs remain stable in the massive parts of lava flows while corrensite and chlorite form in vesicles (Levi *et al.*, 1982; Schmidt & Robinson, 1997). The mineralogical zoning observed in basalt flows has been related to contrasted permeability-porosity properties between vesicular and massive zones (Neuhoff *et al.*, 1999), indicative of different steps in the reaction progress between fluids and rocks. In some cases, not only the mesostasis (supposed to be glassy) but also plagioclases, pyroxenes, and olivines are transformed (albitization or replacement by Mg-rich clay pseudomorphs, respectively). Obviously, the three volcanic bodies studied here have not experienced low-grade metamorphic reactions: no albitization occurred but K-feldspar overgrowths are observed; no corrensite but C-S MLMs and chlorite are present; and Fe-rich smectites are present.

Both the predominance of the Fe-rich clay phases (nontronite-type, Fe-rich saponite, celadonite, chlorite, and all the mixed-layer minerals which include some layers of these minerals) and the absence of corrensite in the three volcanic bodies from Mururoa Atoll indicate that the mineral reactions were controlled chemically by the rock composition. Indeed, the high Fe_2O_3/MgO ratio in the hawaiitic rocks investigated in this work (~3.2), more than twice as high as that of the basalt lava flow from the same magmatic series of Mururoa (Maury *et al.*, 1992), may have promoted the crystallization of rather Fe-rich clay minerals phases. Such a chemical control seems particularly marked in the massive inner parts of the basalts studied. In the same way, no Fe-rich variety of corrensite has been characterized to date, and several authors have suggested that corrensite is a mineral phase that differs chemically from the combined composition of chlorite and smectite layers by a unique compositional range characterized by a rather high Mg/(Mg + Fe) ratio (Shau *et al.*, 1990; Inoue and Utada, 1991; Beaufort *et al.*, 1997).

The nontronite-celadonite problem

The mineralogical composition of the clay fractions extracted from the chilled margins and the massive inner parts are rather similar (Table 4). All contain both trioctahedral and Fe-rich dioctahedral species. The trioctahedral clay species are dominated by Fe-saponite or mixed-layer saponite-chlorite, the dioctahedral species by nontronite-like smectites and/or celadonite. However, in spite of this apparent homogeneity, the clay fractions exhibit some differences, in particular, the

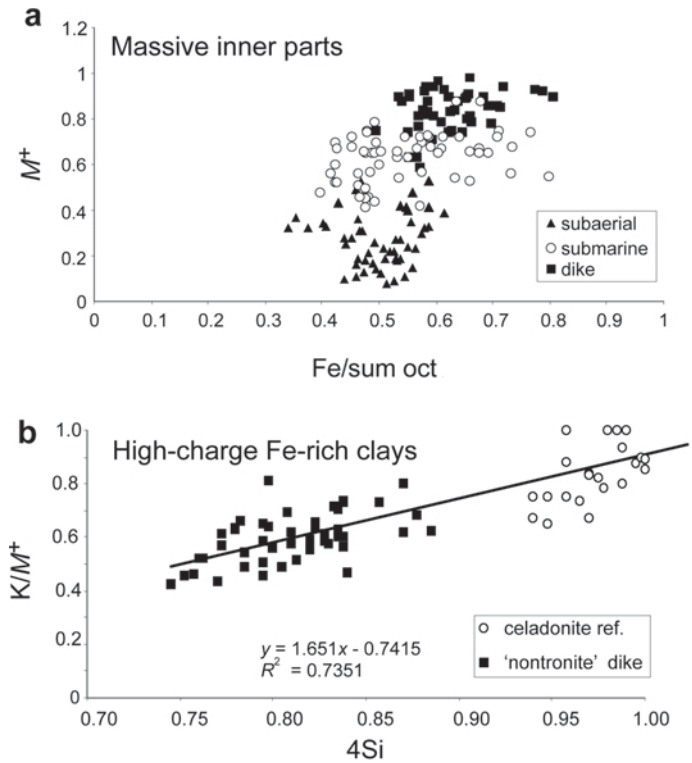

Figure 14. Chemical composition of clay mineral assemblages from the massive inner parts. (a) Plot in the M^+/4Si *vs.* Fe/sum oct coordinates for the three volcanic bodies (microprobe analyses). (b) Comparison in the K/M^+ *vs.* 4Si plot of the high-charge Fe-rich clays (nontronite-like smectites) from the dike with typical basalt celadonites (Foster, 1969; Buckley *et al*., 1978).

celadonite or mixed-layer nontronite-celadonite do not exist in the quenched margins of the subaerial or submarine flows. These phases are associated with Fe-saponite and/or chlorite. Plotted in an M^+/4Si *vs.* Fe/sum oct diagram, the chemical compositions of clay minerals from mesostasis form a continuous field limited by the celadonite-high-charge nontronite-like smectite and chlorite end-members (Figure 14a).

The Fe-rich phases obviously do not fit with the theoretical nontronite field. Their layer charge averages 1 per Si_4O_{10}, making them close to 'celadonite-type' clays. That celadonite does not form is probably related to local chemical conditions such as excess Al and lack of K. The K deficiency is demonstrated in the K/M^+ *vs.* 4Si plot (Figure 14b) because nontronite crystals in the mesostasis are shown to have the same layer charge as typical celadonites (Foster, 1969; Buckley *et al.*, 1978).

CONCLUSIONS

The clay assemblages in the quenched margins and the massive inner parts of the three volcanic bodies studied are polyphasic. In particular, they all contain either pure phases (nontronite-like smectite, celadonite) or mixed-layer minerals formed of expandable and/or non-expandable Fe-rich dioctahedral layers (Table 4). Formed through the alteration of glass in the quenched margins, they are systematically associated with zeolites. In the massive inner parts of the subaerial flow and the dike, these clays are associated with K-feldspar. No evidence was found for albite, corrensite, or mineral zoning between the quenched margins and the massive inner part of the three volcanic bodies. The trioctahedral phyllosilicate sequence, which is typical of hydrothermal alteration or low-grade metamorphism, is not detectable because the Mg-rich phases are composed of randomly ordered C-S MLMs co-existing with chlorite. Consequently, the subaerial and submarine flows and the dike probably have not experienced low-grade metamorphic conditions in spite of their position inside the Mururoa sea-mount. The question is: do the clays formed in the mesostasis of the massive inner part of each body result from the hydrothermal alteration of a basaltic glass as is the case in their quenched margins? This problem will be addressed in a related work (Meunier *et al*., 2008).

The systematic presence of a high-charge nontronite-like smectite makes the Mururoa basalt-hawaiite system a potential terrestrial analog for Mars-surface exploration. Determination of the process which controls the formation of the Fe-rich clays is of great importance in determining the origin of their equivalents on Mars. Thus, the challenge is to confirm the presence of flowing liquid water during the early history of that planet.

ACKNOWLEDGMENTS

This study was supported financially by the University of Poitiers (France) and the 'Institut National des Sciences de l'Univers' (INSU-CNRS). The authors are grateful to anonymous referees and to the editorial team whose suggestions improved the manuscript.

REFERENCES

Alt, J.C. (1999) Very low-grade hydrothermal metamorphism of basic igneous rocks. Pp. 169–201 in: *Low-grade Metamorphism* (M. Frey and D. Robinson, editors). Blackwell Science Ltd, Oxford, UK.

Bardintzeff, J.M., Demange, J., and Gachon, A. (1986) Petrology of the volcanic bedrock of the Mururoa atoll (Tuamotu Archipelago, French Polynesia). *Journal of Volcanology and Geothermal Research*, **28**, 55–83.

Beaufort, D. and Meunier, A. (1994) Saponite, corrensite and chlorite-saponite mixed-layers in the Sancerre-Couy deep drill-hole (France). *Clay Minerals*, **29**, 47–61.

Beaufort, D., Baronnet, A., Lanson, B., and Meunier, A. (1997) Corrensite: a single phase or a mixed layered phyllosilicate of the saponite to chlorite conversion series? The case study of Sancerre-Couy deep drill hole (France). *American Mineralogist*, **82**, 110–125.

Bettison-Varga, L. and Mackinnon, I.D.R. (1997) The role of randomly mixed-layered chlorite/smectite in the transformation of smectite to chlorite. *Clays and Clay Minerals*, **45**, 506–516.

Bettison, L.A. and Schiffman, P. (1988) Compositional and structural variations of phyllosilicates from the Point Sal ophiolite, California. *American Mineralogist*, **73**, 62–76.

Bevins, R.E., Robinson D., and Rowbotham, G. (1991) Compositional variations in mafic phyllosilicates from regional low grade metabasites and application of the chlorite geothermometer. *Journal of Metamorphic Geology*, **9**, 711–721.

Buckley, H.A., Bevan, J.C., Brown, K.M., Johnson, L.R., and Farmer, V.C. (1978) Glauconite and celadonite: two separate mineral species. *Mineralogical Magazine*, **42**, 373–382.

Caroff, M. (1992) Géochimie et pétrologie des roches volcaniques des forages d'Eiao et de Mururoa (Pollynésie Française): approche des processus de genèse et d'évolution des magmas basaltiques en contexte intraplaque océanique. PhD thesis, Université Bretagne Occidentale, Brest, France, 392 pp.

Cox, K.G., Bell, J.D., and Pankhurst, R.J. (1979) *The Interpretation of Igneous Rocks*.: George Allen & Unwin, London, 450 pp.

Desprairies, A., Tremblay, P. and Laloy, C. (1989) Secondary mineral assemblages in a volcanic sequence drilled during ODP leg 104 in the Norwegian Sea. Pp. 397–409 in: *Proceedings of the ODP Scientific Results 104* (O. Eldhom, J. Thiede, E. Taylor *et al*., editors). Texas A&M University, Texas, USA.

Dudoignon, P., Proust, D., and Gachon, A. (1997) Hydrothermal alteration associated with rift zones at Fangatauffa atoll (French Polynesia). *Bulletin of Volcanology*, **58**, 583–596.

Foster, M.D. (1969) Studies of celadonite and glauconite. *U.S. Geological Survey Professional Paper*, **614-F**, 1–17.

Inoue, A. and Utada, M. (1991) Smectite-to-chlorite transformation in thermally metamorphosed volcanoclastic rocks in the Kamikita area, northern Honshu, Japan. *American Mineralogist*, **76**, 628–640.

Köster, H.M., Ehrlicher, U., Gilg, A., Jordan, R., Murad, E., and Onnich, K. (1999) Mineralogical and chemical characteristics of five nontronites and Fe-rich smectites. *Clay Minerals*, **34**, 579–599.

Lanson, B. (1997) Decomposition of experimental X-ray diffraction patterns (profile fitting): a convenient way to study clay minerals. *Clays and Clay Minerals*, **45**, 132–146.

Levi, B., Aguirre, L., and Nystrom, J.O. (1982) Metamorphic gradients in burial metamorphosed vesicular lavas. Comparison of basalt and spilite in Cretaceous basic flows from central Chile. *Contributions to Mineralogy and Petrology*, **80**, 49–58.

Marshall, D.J. (1988) *Cathodoluminescence of Geological Materials*. Unwin Hyman, London.

Maury, R.C., Caroff, M., Achard, S., Guille, G., Joron, J.L., Gachon, A., Rocaboy, A., and Leterrier, J. (1992) L'Atoll de Mururoa (Polynésie Française). La série magmatique. *Bulletin de la Société Géologique de France*, **163**, 659–679.

Meunier, A. (2005) *Clays*. Springer, Heidelberg, Germany.

Meunier, A., Inoue, A., and Beaufort, D. (1991) Chemiographic analysis of trioctahedral smectite-to-chlorite conversion series from the Ohyu Caldera, Japan. *Clays and Clay Minerals*, **39**, 409–415.

Meunier, A. and El Albani, A. (2007) The glauconite-Fe-illite-Fe-smectite problem: a critical review. *Terra Nova*, **19**, 95–104.

Meunier A., Mas, A., Beaufort, D., Patrier, P., and Dudoignon, P. (2008) Clay minerals in basalt-hawaiite rocks from Mururoa atoll (French Polynesia). II. Petrography and geochemistry. *Clays and Clay Minerals*, **56**, 730–750.

Neuhoff, P.S., Fridriksson, T., Anorsson, S., and Bird, D.K. (1999) Porosity evolution and mineral paragenesis during low-grade metamorphism of basaltic lavas at Teigarhorn, eastern Iceland. *American Journal of Science*, **299**, 467–501.

Odom, I.E. (1984) Glauconite and celadonite minerals. Pp. 545–572 in: *Micas* (S.W. Bailey editor), **13**, Mineralogical Society of America, Washington, D.C.

Reynolds, R.C. (1985) *NEWMOD, a computer program for the Calculation of one-Dimensional Diffraction of Mixed-layer Clays*. R.C. Reynolds Jr., 8 Brook Dr., Hanover, New Hampshire, USA.

Shau. Y.H., Peacor, D., and Essene, E. (1990) Corrensite and mixed layer chlorite/corrensite in metabasalts of northern Taiwan: TEM/AEM, EPMA, XRD, and optical studies. *Contributions to Mineralogy and Petrology*, **105**, 123–142.

Schiffman, P. and Day, H.W. (1999) Petrological methods for the study of very low-grade metabasites. Pp 108–142 in: *Low-grade Metamorphism* (M. Frey and D. Robinson, editors). Blackwell Scientific, Oxford.

Schiffman, P. and Fridleifsson, G.O. (1991) The smectite–chlorite transition in drillhole NJ-15, Nesjavellir geothermal field, Iceland: XRD, BSE and electron microprobe investigations. *Journal of Metamorphic Geology*, **9**, 679–696.

Schmidt, S.T. and Robinson, D. (1997) Metamorphic grade and porosity and permeability controls on mafic phyllosilicate distributions in a regional zeolite to greenschist facies transition of the North Shore Volcanic Group, Minnesota. *Geological Society of America Bulletin*, **109**, 683–697.

Thorpe, R.S. and Smith, K. (1975) Midplate volcanism. Pp. 75–80 in: *Geodynamics Today, a Review of Earth's Dynamic Processes.* Royal Society, London.

(*Received 8 April 2008; revised 12 September 2008; Ms. 0124; A.E. W. Huff*)